Journal of NAMP 70, (2025) 67-78

The Nigerian Association of Mathematical Physics

Journal homepage: https://nampjournals.org.ng

FIRST PRINCIPLES INVESTIGATION OF HALF-METALLIC MgSrB AND MgSrAl

Obiahu, S. C. and Nenuwe N. O.

Department of Physics, Federal University of Petroleum Resources Effurun, Nigeria.

ARTICLE INFO

Article history:
Received 16/5/2025
Revised 9/6/2025
Accepted 10/6/2025
Available online 17/7/2025

Keywords:
Optical properties, Structural properties, Electronic properties, MgSrAl, Wien2k.

ABSTRACT

A comprehensive study on optical, electronic and structural properties for MgSrB and MgSrAl has been conducted using density functional theory (DFT). The computations predict that MgSrB and MgSrAl are half-metallic compounds. The band gap in the up spin channel is 0.826 and 1.263 eV with PBE-GGA and mBJ for MgSrB. While, for MgSrAl, gap in the up spin channel is 0.477 eV with mBJ, and it is a spin-gapless semiconductor with PBE-GGA approximation. The optical properties of MgSrB and MgSrAl alloy were also examined, and the imaginary component of the dielectric function exhibits pronounced absorption peaks within the energy spectrum of 0.149 – 4.993 eV for the both alloys. These peaks result from transitions among different states of ions and atoms in these compounds. In general, our results indicate that MgSrB and MgSrAl half-Heusler alloys are good materials for optoelectronics, solar cells and spintronics.

1. INTRODUCTION

Extensive exploration has been focused on Heusler-based compounds due to their fascinating and versatile properties. Heusler compounds consist of mainly two types: full-Heusler and half-Heusler (h-H). They are represented by the chemical formulas X_2YZ and XYZ, respectively. In these formulations, Z represents the main group element that acts as the anion, while Y and X are metallic elements with different charges. Semiconductor Heusler compounds are highly appealing due to their significant prospect in several applications such as spintronics, diluted magnetic solar cells, semiconductors, topological insulators, thermoelectrics, and more [1-3]. Various methods have been employed to synthesise half-Heuslers. For example, CoTiSb is grown using molecular beam epitaxy [4], TiNiSn is synthesised through spark plasma sintering, ball-milling, and arc-melting [5], nanostructured half-Heusler NbFeSb alloy is created by mechanical alloying, and TmNiSb is synthesized through arc-melting, high-pressure, and high-temperature method [6].

*Corresponding author: NENUWE N. O.
E-mail address: nenuwe.nelson@fupre.edu.ng
https://doi.org/10.60787/jnamp.vol69no2.536

Most h-H compounds, with the chemical formulation XYZ, exhibit either a cubic F-43m half-Heusler structure (for example, PtZrSn and PtHfSn [7]), and a hexagonal structure (for example, LiAlSi [8] and TmNiSb [6]). Several XYZ compounds contain both hexagonal and cubic phases [9]. In recent theoretical research, it has been determined that RhTiP is semiconductor with an indirect band gap (Eg) of 1.027 eV using the TB-mBJ method [10]. In addition, LiSrP has a direct band gap, while LiSrAs exhibits an indirect band gap [11]. The PtZrSn and PtHfSn possess indirect bandgap semiconductor characteristic. The PtHfSn and PtZrSn compounds have bandgaps of 0.94 eV and 1.23 eV, respectively [7]. The RbSrGe and RbSrSn alloys have been shown to exhibit half-metallic behaviour [12]. The optical property measurements in Ref. [11] indicate that LiSrAs and LiSrP have significant absorption and minimal reflection in the visible and low ultraviolet (UV) bands. It has been determined that RuVBi has significant absorption coefficient [13]. The Eg of the NbFeSb compounds is determined to be 0.37 eV from the analysis of UV-Vis absorbance spectra using a Tauc plot. The reflectance of BaAgP stays nearly stable from the visible to UV range 1.65-12 (eV), as indicated in Reference [14]. At 340 K, TiRuSb half-Heusler displays a unique glass-like thermal transport behaviour and possesses the least lattice thermal conductivity (κ_L), measuring approximately 1.65 $Wm^{-1}K^{-1}$, among the previously known h-H phases [15]. RhTiP exhibits an electronic figure of merit (ZTe) of 0.25 eV at ambient temperature and a maximal Seebeck coefficient (Sbc) of 1380 μV/K [10]. The Sbc for n-type doped LiSrP was measured to be 3116.46 μV/K, while for LiSrAs it was found to be 3055 μV/K. At a temperature of 300K, the ZT reaches a peak of 0.98, as stated in reference [11]. Ref. [7] reports a low κ_L at ambient temperature for PtZrSn (16.96 W/mK) and PtHfSn (10.04 W/mK) compounds. The PtHfSn material has a ZTe of 0.57, whereas the PtZrSn material has a ZT of 0.24. In addition, the thermoelectric properties of TiNiSn were enhanced by including Cu. At a temperature of 773 K, a ZT of 0.6 was achieved, which is the highest value obtained [5]. On the other hand, the thermoelectric properties were estimated by utilizing the semi-classical Boltzmann transport theory in the BoltzTraP [17]. The ab initio method was employed in the theoretical investigation to ascertain the optical and electronic characteristics of BaHgSn [16]. The study was conducted to address the research gaps in the physical features of BaHgSn material, and it provided innovative approaches for beginners. In addition, the thermoelectric features of FeVTe and FeTiSe [18,19] were predicted by Boltzmann transport theory. Their work aimed to fill the research gaps regarding the physical characteristics of FeVTe and FeTiSe materials, supplying data on these novel Fe-based compounds.

Recently, an imperative family of compounds without a transition metals have garnered the interest of researchers. These sp-compounds are known to exhibit half metallic behavior and finds applications in spintronic devices. More recently, BeSrB and MgSrB were predicted to exhibit half metallicity [20]. In their study, the researchers employed the first principles technique to analyze the structural, elastic, electronic and magnetic properties of BeSrB and MgSrB half Heuslers. They envisaged that these materials have the potential for spintronic applications. However, they do not study the optical properties and dynamical stability of these materials. These significant findings motivate us to hunt for novel half Heuslers that are free from transition metals but possess half metallicity. In this study, two magnesium-based h-H compounds MgSrB and MgSrAl are examined. To the best of our knowledge, there is no study on the physical properties MgSrAl alloy. Therefore, in this research work, we have provided the missing knowledge on the physical characteristics of MgSrB and MgSrAl , by studying the properties of these two alloys paying special interest to the optical properties alongside with the structural stability, and electronic properties. We adopt the first principles computations built on DFT as configured in the WIEN2K computational code.

2. Materials and Methods

In this work, we have used the Wien2k Software Package for the computations of the electronic, structural, and optical properties of MgSrB and MgSrAl half-Heusler compounds. The FP-LAPW technique [21], executed in the Wien2k [22], was engaged to execute DFT [23] computations on MgSrB and MgSrAl alloys. We employ the PBE functional to analyze the exchange-correlation potential. In our investigations, we utilize spin-polarized DFT to exactly consider the optimization of electronic structures since MgSrB and MgSrAl are ferromagnetic alloys. The energy convergence limit was set to 10^{-5} Rydberg, whereas the charge convergence threshold was kept at 10^{-4} e, where '*e*' represents the charge of an electron. The value of $R_{MT}K_{max}$ was taken as 8 for the alloys to restrict the quantity of plane waves. R_{MT} signifies the Muffin-Tin Radius and K_{max} represents the highest value chosen for the expansion of the entire plane wave vector. The wave functions are allowed to expand in the muffin-tin spheres to the maximum angular momentum value, $l_{max} = 10$. Considering that G_{max} is the biggest vector value in charge density, its magnitude was set to 12 $(a.u)^{-1}$. In addition, in order to prevent the spheres from overlapping, the Rmt values for the Mg, Sr, Al, and B atoms were set to 2.14 and 2.08. A cutoff energy of -6.0 Ryd was selected to define the separation of valence and core states within the muffin tin. The computations were performed using a total of 2000 k-points in the Brillouin zone to build the charge density in each self-consistency step.

3. Results and Discussion

3.1. Structure Properties

The primary procedure in any first principles analysis is the identification and analysis of the structural features of the compounds. This knowledge enables us to determine other characteristics of the compounds, such as optical and electronic properties. MgSrB and MgSrAl half-Heuslers have a conventional formula of XYZ, where Z is B and Al, Y is Sr and X is Mg atom. It is well known that to formulate half-Heuslers there are basically three possibilities to fill the atomic sites: α, β, and γ phase. In the α phase, XYZ occupies (0.25, 0.25, 0.25) (0.75, 0.75, 0.75) (0, 0, 0); β phase XYZ takes (0, 0, 0) (0.75, 0.75, 0.75) (0.25, 0.25, 0.25), and in the γ phase (0.5, 0.5, 0.5) (0.75, 0.75, 0.75) (0, 0, 0).

Usually, half-Heuslers are most likely to be stable in α-phase. This was confirmed in this work through the structural optimization of our compounds under investigation as shown in Figure 1. For this reason, we have investigated the structural properties alongside the optical and electronic properties in the α-phase where the Mg, Sr, and B(Al) atoms occupy the atomic positions (0.25, 0.25, 0.25), (0.75, 0.75, 0.75) and (0, 0, 0), respectively. It is vital to note that the α-phase is a structure with F43m space group (no. 216). Ferromagnetic (FM) and non-magnetic (NM) states were investigated, and both compounds are stable in the FM states. Figure 2 represents the conventional unit cell of MgSrB and MgSrAl compounds in α-phase. The B-atom is bonded by both Sr and Mg atoms, whereas the Sr atoms are positioned between two atoms of Mg in the α-phase for MgSrB. In the MgSrAl compound, the Al-atom is bonded to both Sr & Mg, with Sr located between atoms of Mg. The total energy of MgSrB and MgSrAl was evaluated as a function of volume in the alpha-phase, and we plotted energy versus volume in Figure 3.

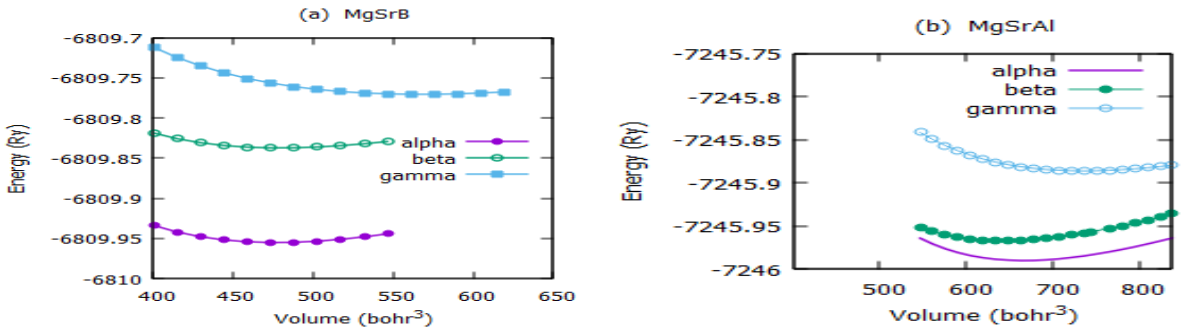

Fig. 1. Energy versus volume for (a) MgSrB and (b) MgSrAl within the alpha, beta and gamma structural phase.

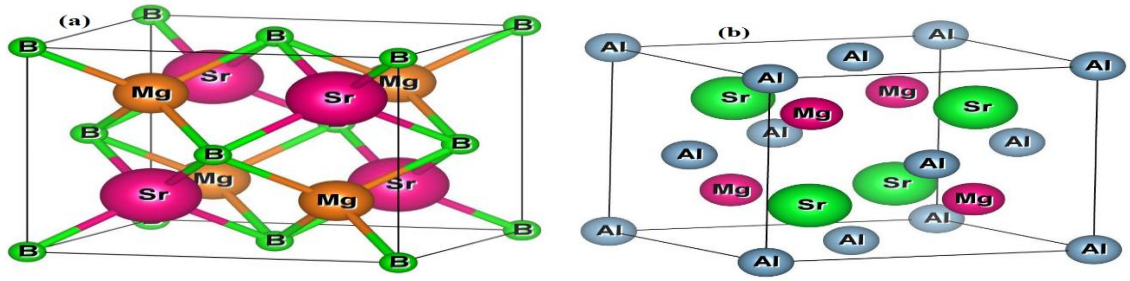

Fig. 2. The structure of (a) MgSrB and (b) MgSrAl alloy

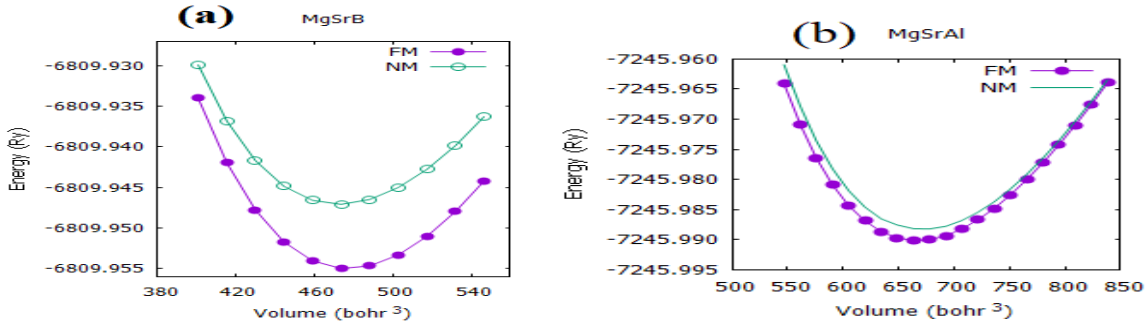

Fig. 3. Energy versus volume for (a) MgSrB and (b) MgSrAl within ferromagnetic (FM) and non-magnetic (NM) states.

To ascertain the equilibrium lattice constant, and other structural parameters of MgSrB and MgSrAl, this graph was fitted to the Murnaghan equation of states given in Equation (1).

$$E_T(V) = E_0 + \frac{B_0 V}{B_0'(B_0'-1)}\left\{\left(\left(\frac{V_0}{V}\right)^{B_0'} - 1\right) + B_0'\left(1 - \frac{V_0}{V}\right)\right\} \qquad (1)$$

where B_0 & B'_0 remain bulk modulus and its derivative in equilibrium volume (V_0). E_0 is equilibrium energy. The calculated results for the lattice constant (a_0), B_0 and B'_0 for MgSrB and MgSrAl are recorded in Table 1. Our calculated results for the lattice constant, bulk modulus and its pressure derivative are in agreement with the previously reported results [20] for MgSrB. However, results obtained for MgSrAl are appearing for the first time in the literature. Therefore,

the predicted structural data for MgSrAl can be used as basis for both experimental and theoretical studies for this material.

In order to predict the possible experimental synthesis of these materials, the formation energy (E_f) for each compound is computed using the equation:

$$E_f = E_T^{MgSrB(Al)} - E_T^{Mg} - E_T^{Sr} - E_T^{B(Al)} \quad (2)$$

where E_T^{Mg}, E_T^{Sr} *and* $E_T^{B(Al)}$ are the bulk total energies of Mg, Sr, and B(Al). E_T^{MgSrB} is the total energy of MgSrB. The predicted data of formation energy are recorded in Table 1. We observed that the E_f of MgSrAl and MgSrB in the alpha phase with FM state is negative and thus both materials under study are thermodynamically stable and suggests the possibility of their experimental fabrication. The obtained value of formation energy for MgSrB is agreement with that reported by Abada *et al* [20].

Table 1. Calculated structural parameters of MgSrB and MgSrAl alloys.

Alloy	a_0 (Å)	B (GPa)	B'	V_0 (bohr^3)	E_T (Ry)		E_f (Ry)	E_g(Ry)
	FM	FM	FM	FM	FM	NM		
MgSrB	6.56 6.563[20]	38.60 38.742[20]	3.52 3.69[20]	477.28	-6809.954988	-6809.947066	-0.81 -0.798[20]	0.826 (GGA) 1.263 (mBJ) 0.831 (GGA) [20] 1.277 (mBJ) [20]
MgSrAl	7.35	25.78	3.21	669.95	-7245.990303	-7245.988282	-0.0032	0.00 (GGA) 0.447 (mBJ)

3.2. Electronic Analysis

3.2.1. Band Structure

Here, we have computed and plotted the band structures of MgSrB and MgSrAl alloys employing PBE-GGA and mBJ approximations. Spin-polarized calculations were calculated for the examination of the electronic properties. Figure 4 describes the band structure analysis with PBE-GGA and mBJ. We observe, from these plots, in the spin-down channel, there is an overlapping at the Fermi energy (E_F) levels between the minimum position of the conduction band (CBM) and the maximum position of the valence band (VBM) for both MgSrB and MgSrAl. With the mBJ approximation, we observe a slight shift of the CBM and VBM upwards and downwards for both materials along the down-spin channel. In both plots, there is no gap, hence, both materials have metallic character in the down spin direction. In the spin-up channel, with PBE-GGA approximation, the VBM lies along the Fermi energy levels for MgSrAl, there is no gap. Hence, this alloy exhibits metallic character along spin-up direction with PBE-GGA approximation. With the mBJ approximation, along the spin-up, we noticed that the VBM shifts downward for MgSrAl, creating a gap between the CBM and VBM, the alloy exhibits semiconductor character. This indicates that MgSrAl compound is a half-metallic material with the mBJ approximation. But with the PBE-GGA approximation MgSrAl is a metallic material. For MgSrB alloy, in the up spin direction, with both PBE-GGA and mBJ approximations, we observe a clear band gap, hence, it behaves as a semiconductor along this channel. This suggests that MgSrB is half-metallic material with both approximations, hence, it may be suitable for spintronic applications. As represented in Figure 5 in the up spin path, the direct band gap (E_g) along the XX symmetry are 0.826 eV and

1.263 eV with PBE-GGA and mBJ, respectively. Whereas, in the up-spin channel, with mBJ approximation, MgSrAl manifest as an indirect band gap (E_g) along ΓX symmetry, with energy band gap of 0.477 eV. Our results clearly show that the band gap values obtained with mBJ are larger than values obtained with PBE-GGA. The mBJ approximations are known to predict band gap values that are very close to experimentally generated data. Our results obtained for band gap are in agreement with the previously reported values for both GGA and mBJ approximations for MgSrB.

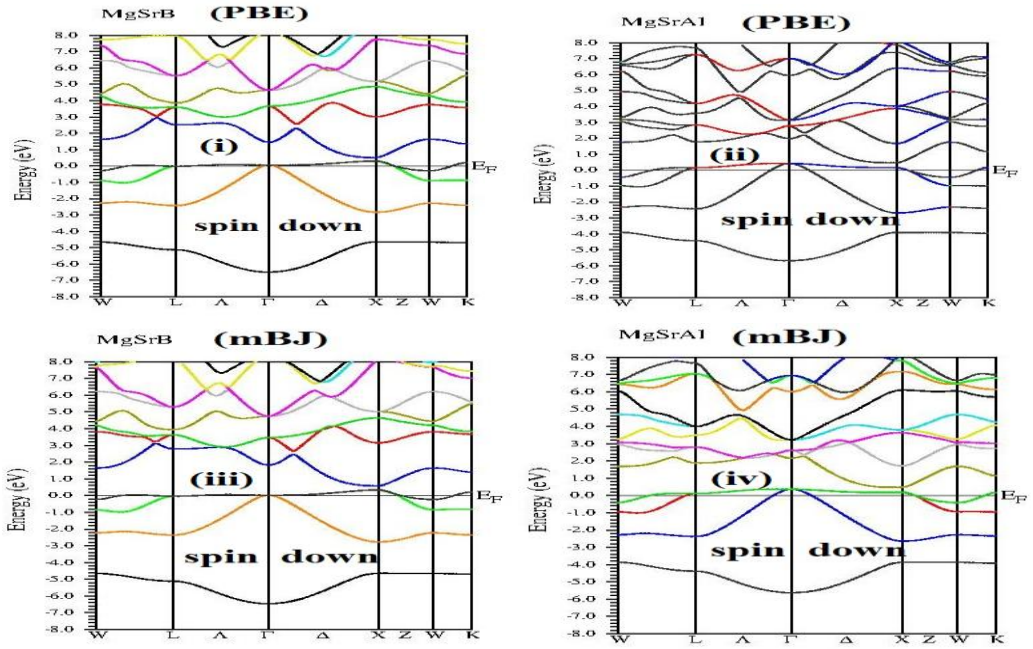

Fig. 4. Band structure of down-spin channel for MgSrB (i & iii) and MgSrAl (ii & iv) using PBE-GGA and mBJ approximations.

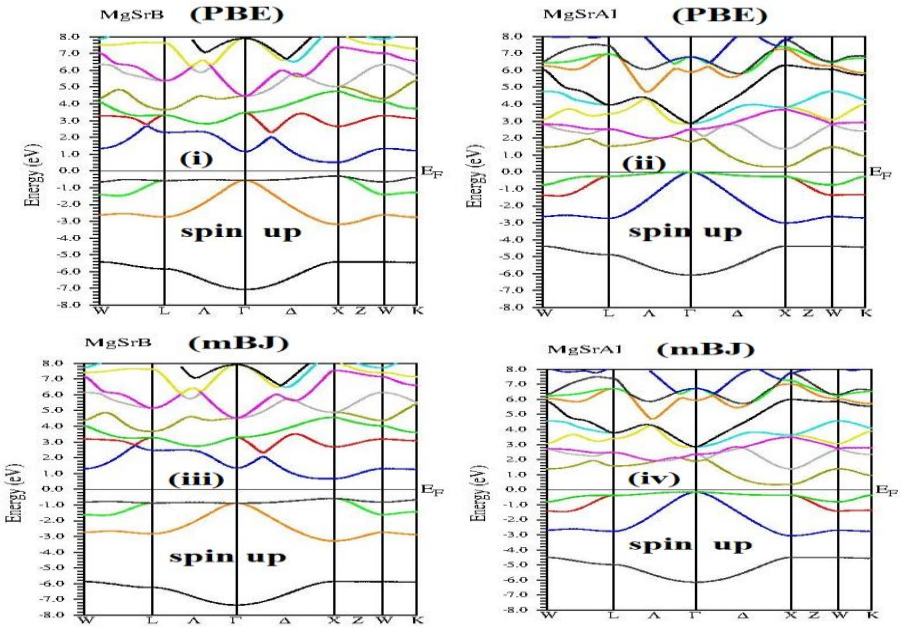

Fig. 5. Band structure of up-spin channel for MgSrB (i & iii) and MgSrAl (ii & iv) using PBE-GGA and mBJ approximations.

3.2.2 Density of States

To comprehend contributions to the band gap, we have evaluated the total density of states (T-DOS) and partial density of states (P-DOS) as reported in Figures 5 and 6 for MgSrB and MgSrAl using mBJ approximations. The contributions from each atom to the band gap are represented in Figure 6. Our findings are: (i) T-DOS for both compounds are similar due to the similarity in their crystal structure. (ii) For both compounds, there is an overlap of the bands with the E_F in the down-spin path, while for the up-spin direction, there is no overlap of the DOS with the E_F. This indicates the existence of a band gap in the majority channel. Hence, both MgSrB and MgSrAl are half-metallic materials. (iii) The density of states for *s*-orbital are smaller than those of *p*-orbital. (iv) The *p*-orbital from boron (B) atoms dominate the region around Fermi Level for MgSrB. (v) In MgSrAl, *p*-Al orbital has the dominant contribution to the band gap, whereas the *s*-orbitals have minimal contribution. The contributions from *s & p* bands from each atom can be viewed in Figure 7(i-iv) and Figure 8(i-iv), respectively.

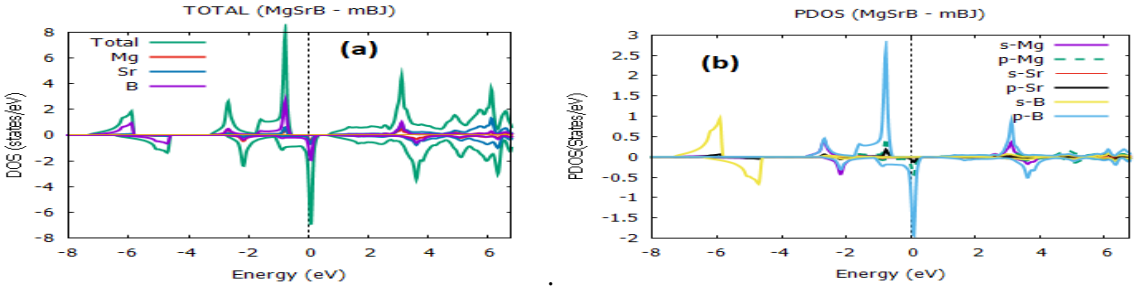

Fig. 6. (a) Total density of states and (b) partial density of states for MgSrB with mBJ approximation

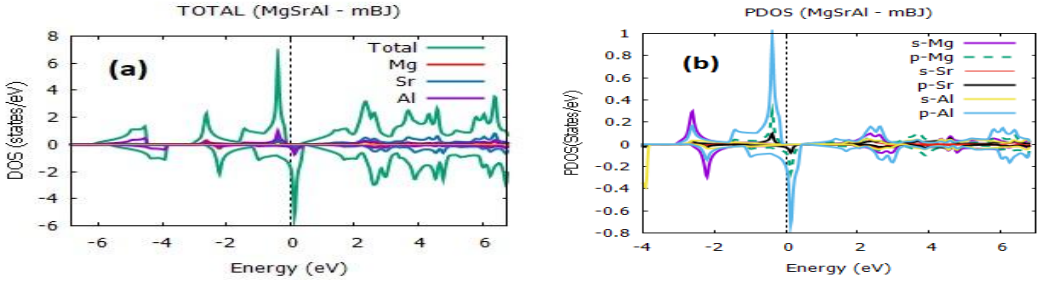

Fig. 7. (a) Total density of states and (b) partial density of states for MgSrAl with mBJ approximation

3.3. Magnetic Properties

As reported in Table 2, we examined the partial magnetic moments of Mg, Sr, B, and Al atoms and contributions of interstitial region. The majority impact to total magnetic moment M_{tot} is from boron B atom for MaSrB, and from interstitial region for MgSrAl alloy. The computed M_{tot} for the alloys is an integer of 1 per formula unit which follows the Slater-Pauling rule for 8-valence electron count: $M_{tot} = (Z_{tot}\text{-}8)\ \mu_B$ where Z_{tot} is the total number of valence electrons. Usually, for half-metallic half-Heuslers with less than 8 electrons such as our compounds, the energy gap is in the spin-up band and not in the spin-down band. In fact, an appropriate relation is $M_{tot} = (8\text{-}\ Z_{tot})\ \mu_B$, where $Z_{tot} = 7$ for both compounds, with 2 from Mg-atom, 2 from Sr-atom and 3 electrons from B or Al-atom. This results to a M_{tot} of 1 μ_B per unit cell. This is in perfect agreement with our calculated value for M_{tot}. The calculated magnetic moments for MgSrB are in good agreement with previous results [2].

Table 2. Computed magnetic moment in μ_B, the Mg atom moment (M_{Mg}), Sr atom moment (M_{Sr}), B atom moment (M_B), Al atom moment (M_{Al}), interstitial moment (M_{int}), and total magnetic moment (M_{tot}) for MgSrB and MgSrAl.

Magnetic moment (μ_B)	MgSrB	MgSrAl
M_{Mg}	0.02362	0.03598
M_{Sr}	0.05068	0.05412
M_{int}	0.44067	0.72692
M_B	0.48504	-
M_{Al}	-	0.18305
M_{tot}	1.0000	1.0000
	1.000 [20]	

3.4. Optical Properties

The optical characteristics of solid materials represent quantifiable physical properties that can be examined through the computations of the photon-dependent dielectric function, which is intrinsically linked to the electronic bandstructure. The dielectric function, encompassing both its imaginary and real components, comprehensively reveals the diverse optical features exhibited by solids [24]. The examination of these characteristics is essential for predicting the appropriateness of solids for potential applications. Consequently, the dielectric function $\varepsilon(\omega) = \varepsilon_1(\omega) + i\varepsilon_2(\omega)$ has been computed & employed to investigate the optical properties of the MgSrB and MgSrAl materials. The imaginary part $\varepsilon_2(\omega)$ given by Equation (3), serves as a fundamental prerequisite for calculating various optical properties, comprising the absorption spectrum, optical conductivity, refractive index (RI), reflectivity, loss function, and real part of the dielectric function, $\varepsilon_1(\omega)$ of the material.

$$\boldsymbol{\varepsilon_2(\omega) = \frac{4\pi e^2}{m^2 \omega} \int d^k \sum_{n\,n'} |\langle kn|p|kn'\rangle|^2 \times f_{kn}(1 - f_{k'n'}) \delta(E_{kn} - E_{kn'} - \omega\hbar)} \qquad (3)$$

The value of $\varepsilon_1(\omega)$ is derived from the computed spectrum of $\varepsilon_2(\omega)$ through the application of the Kramers-Kronig transformation relation captured in Equation (4) [25]. All additional optical parameters can be derived from $\varepsilon_1(\omega)$ and $\varepsilon_2(\omega)$. The detailed methodology and associated equations for these optical parameters, utilising a FPLAPW as executed in WIEN2k, are also available in the existing literature [25, 26].

$$\boldsymbol{\varepsilon_1(\omega) = 1 + \frac{2}{\pi} \int_0^\infty \frac{\omega' \varepsilon_2(\omega')}{\omega'^2 - \omega^2} \, d\omega} \qquad (4)$$

The refractive index RI(ω), extinction coefficient K(ω) and absorption coefficient (A) are computed with relations in Equations (5), (6) & (7), respectively.

$$RI(\omega) = \left(\frac{\sqrt{\varepsilon_1^2(\omega) + \varepsilon_2^2(\omega)} + \varepsilon_1(\omega)}{2} \right)^{\frac{1}{2}} \qquad (5)$$

$$K(\omega) = \left(\frac{\sqrt{\varepsilon_1^2(\omega) + \varepsilon_2^2(\omega)} - \varepsilon_1(\omega)}{2} \right)^{\frac{1}{2}} \qquad (6)$$

$$A(\omega) = \frac{2\omega K(\omega)}{c} \qquad (7)$$

Figure 8(a-e) show that the compound MgSrB has the utmost real part of the dielectric function $\varepsilon_1(\omega)$ and hence the highest refractive index, optical polarizability, optical reflectivity, and optical absorption coefficient. This is accredited to the remarkable existence of the DOS at the E_F in the down spin channel of MgSrB compound. This allows the charge carrier in MgSrB to move more freely than those in MgSrAl material. The highest optical polarizability of MgSrB is a suitable property for several uses, such as solar cells, optical gadgets and sensors. For instance, the high reflectivity of MgSrB makes it a suitable contender for mirror and other optical modules. The imaginary part $\varepsilon_2(\omega)$ is a measure of how much light a compound can absorb. Figures 7(b & e) demonstrate that intense absorption points occur in the energy range 0.149 – 4.993 eV for both compounds. The dominant peak of both compounds MgSrB and MgSrAl reside in the visible and infrared regions, but the diminishing points falls within the ultra-violet section. The pinnacles of the imaginary parts of the $\varepsilon(\omega)$ are directly related to the absorption of MgSrB and MgSrAl alloys in Figure 8(e). These are imputable to transitions linking unique states of atoms and ions in the alloys. The PDOS in Figure 6(b) offers a way for these transitions. Corresponding to the P-DOS in Figure 8, various electronic transitions might occur from the top of the valence band (VB) to the bottom of the conduction band (CB). Certainly, the gaps from the top of the VB to the bottom of the CB of the Mg, Sr, B, and Al correspond to the transition points in the visible range. Therefore, the absorptions within Figure 6 (e) in the visible range are ascribed to the transition from the top of the VB to the CB of Mg, Sr, B, and Al. The optical reflectivity is related to the absorption coefficient. Optical reflectivity is inversely proportional to the absorption coefficient, indicating that it is minimal when the absorption coefficient is greatest, and vice versa. The RI of a material is a critical measure for photoelectric purposes. The RI of MgSrB and MgSrAl are shown in Figure 8 (d). The RI exhibit peaks and then gradually falls to a minimum value of 0.256 and 0.629 for MgSrB and MgSrAl, respectively, at around 13.565 eV. The peaks originate from the interband transition between the highest VB and lowest CB.

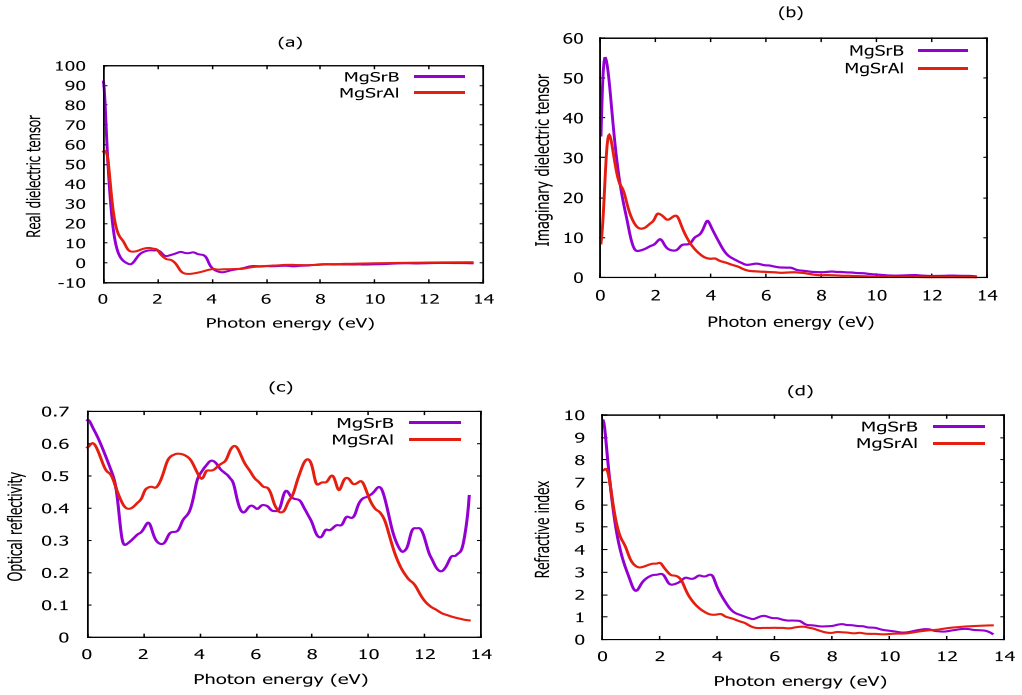

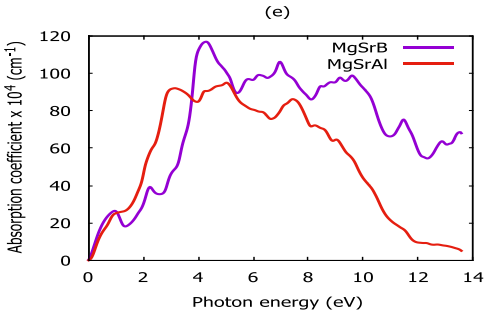

Fig. 8. Optical properties for MgSrB with mBJ Approximation: (a) Real dielectric tensor, (b) Imaginary dielectric tensor, (c) Optical reflectivity, (d) Refractive index, and (e) Absorption coefficient.

Conclusion

We conducted a comprehensive examination of structure, optical & electronic characteristics of half-Heusler MgSrB and MgSrAl materials using density functional theory. Our computations predict that MgSrB and MgSrAl are half-metallic compounds. The band gap in the up spin channel is 0.826 eV and 1.263 eV with PBE-GGA and mBJ for MgSrB. Whereas, for MgSrAl, the band gap in the up spin channel is 0.477 eV with mBJ, and it is a spin gapless semiconducting material with the PBE-GGA approximation. The optical properties of MgSrB and MgSrAl alloy were also investigated. MgSrB exhibits the highest real part of the dielectric function and thus the highest optical polarization, RI and optical reflectivity in the visible range. This is ascribed to the obvious existence of the density of states at Fermi energy in the down spin path of these materials. The imaginary part of the dielectric function shows strong absorption peaks in the energy range of 0.149 – 4.993 eV for MgSrB and MgSrAl alloy. These points are due to transitions between unique states of ions and atoms in these compounds. In general, our results indicate that MgSrB and MgSrAl half-Heusler alloys are favourable materials for optoelectronics, spintronics, and solar cells

Conflict of Interest

The authors declare no conflict of interest.

References

[1] Z. Dong, J. Luo, C. Wang, Y. Jiang, S. Tan, Y. Zhang, Y. Grin, Z. Yu, K. Guo, J. Zhang, and W. Zhang. Half-Heusler-like compounds with wide continuous compositions and tunable p- to n-type semiconducting thermoelectrics. *Nature Communications* 13: 35 (2022). https://doi.org/10.1038/s41467-021-27795-3.

[2] F. Casper, T. Graf, S. Chadov, B. Balke, and C. Felser. Half-Heusler compounds: Novel materials for energy and spintronic applications. *Semiconductor Science and Technology* 27(6): 1-8 (2012). https://doi.org/10.1088/0268-1242/27/6/063001.

[3] N.O. Nenuwe and O. Omagbemı. DFT based Investigation of Structural, Thermodynamic, Mechanical and Electronic Properties of RuVZ (Z: As, Bi, Sb) Half-Heusler Semiconductors. *VNU Journal of Science: Mathematics - Physics* 38(3): 24-37 (2022). https://doi.org/10.25073/2588-1124/vnumap.4705.

[4] J.K. Kawasaki, L.I.M. Johansson, B.D. Schultz, and C.J. Palmstrøm. Growth and transport properties of epitaxial lattice matched half Heusler CoTiSb/InAlAs/InP(001) heterostructures. *Applied Physics Letters* 104: 022109 (2014). https://doi.org/10.1063/1.4862191.

[5] K. Chen, C. Nuttall, E. Stefanaki, K. Placha, R. Tuley, K. Simpson, J.W.G. Bos, and M.J. Reece. Fast synthesis of n-type half-heusler TiNiSn thermoelectric material. *Scripta Materiala* 191: 71-75 (2021). https://doi.org/10.1016/j.scriptamat.2020.09.010.

[6] K. Ciesielski, K. Synoradzki, D. Szymański, K. Tobita, K. Berent, P. Obstarczyk, K. Kimura, and D. Kaczorowski. Half-Heusler phase TmNiSb under pressure: intrinsic phase separation, thermoelectric performance and structural transition. *Scientific Reports* 13: 1592 (2023). https://doi.org/10.1038/s41598-023-28110-4.

[7] S. Ahmad Khandy, K. Kaur, S. Dhiman, J. Singh, and V. Kumar. Exploring thermoelectric properties and stability of half-Heusler PtXSn (X = Zr, Hf) semiconductors: A first principle investigation. *Computational Materials Science* 188: 110232 (2021). https://doi.org/10.1016/j.commatsci.2020.110232.

[8] F. Casper, R. Seshadri, and C. Felser. Semiconducting half-Heusler and LiGaGe structure type compounds. *Physica Status Solidi (A) Applications and Materials Science* 206: 1090-1095 (2009). https://doi.org/10.1002/pssa.200881223.

[9] W. Wong-Ng, and J. Yang. International centre for diffraction data and american society for metals database survey of thermoelectric half-heusler material systems. *Powder Diffraction* 28: 32-43 (2013). https://doi.org/10.1017/S0885715612000942.

[10] S. Dubey, J.A. Abraham, K. Dubey, V. Sahu, A. Modi, G. Pagare, N.K. Gaur, DFT study of RhTiP half Heusler semiconductor: Revealing its mechanical, optoelectronic, and thermoelectric properties, *Physica B: Condensed Matter* 672: 415452 (2024). https://doi.org/10.1016/J.PHYSB.2023.415452.

[11] A. Azouaoui, A. Harbi, M. Moutaabbid, M. Idiri, A. eddiai, N. Benzakour, A. Hourmatallah, K. Bouslykhane, R. Masrour, and A. Rezzouk. First-principle investigation of LiSrX (X=P and As) half-Heusler semiconductor compounds. *Indian Journal of Physics* 97: 1727-1737 (2023). https://doi.org/10.1007/s12648-022-02522-w.

[12] N.O. Nenuwe, J.O. Umukoro, and E.A. Enaibe. First-principles calculations to investigate structural, electronic, magnetic, thermodynamic, and thermoelectric properties of RbSrZ (Z = Ge and Sn) d0-d0 half-Heuslers for renewable energy applications. *Kuwait Journal of Science* 52: 100300 (2025). https://doi.org/10.1016/J.KJS.2024.100300.

[13] N.O. Nenuwe, and J.O. Umukoro. TB-mBJ Predictions of Thermoelectric and Optical Properties of Half-Heusler RuVBi alloy. *FUPRE Journal of Scientific & Industrial Research* 7: 55–70 (2023). http://fupre.edu.ng/journal.

[14] F. Parvin, M.A. Hossain, I. Ahmed, K. Akter, and A.K.M.A. Islam. First-principles calculations to investigate mechanical, optoelectronic and thermoelectric properties of half-Heusler p-type semiconductor BaAgP. *Results in Physics* 23: 104068 (2021). https://doi.org/10.1016/j.rinp.2021.104068.

[15] Z. Dong, J. Luo, C. Wang, Y. Jiang, S. Tan, Y. Zhang, Y. Grin, Z. Yu, K. Guo, J. Zhang, and W. Zhang. Half-Heusler-like compounds with wide continuous compositions and tunable p-

to n-type semiconducting thermoelectrics. *Nature Communications* 13: 35 (2022). https://doi.org/10.1038/s41467-021-27795-3.

[16] G.K.H. Madsen, J. Carrete, and M.J. Verstraete. BoltzTraP2, a program for interpolating band structures and calculating semi-classical transport coefficients. *Computer Physics Communications* 231: 140-145 (2018). https://doi.org/10.1016/j.cpc.2018.05.010.

[17] A. Jabar, S. Benyoussef, and L. Bahmad. A first principal study of the electronic, optic and thermoelectric properties of double perovskite K2CuRhX6 (X = Cl or I). *Optical Quantum Electrons* 55: 839 (2023). https://doi.org/10.1007/s11082-023-05130-y.

[18] N.O. Nenuwe, and A.S. Yebovi. Predictive analysis of a new FeVTe alloy from first principles: An excellent choice for thermoelectric applications. *Computational Condensed Matter* 38: e00882 (2024). https://doi.org/10.1016/j.cocom.2024.e00882.

[19] N.O. Nenuwe, and N.O. Agbawe. Ab initio predictions of thermoelectric, mechanical, and phonon characteristics of FeTiSe half-Heusler compound. *Current Applied Physics* 53: 132-141 (2023). https://doi.org/10.1016/j.cap.2023.06.008.

[20] A. Abada, N. Marbouh, and A. Bentayeb. First-principles calculations to investigate structural, elastic, electronic and magnetic properties of novel d0 half metallic half Heusler alloys XSrB (X= Be, Mg). *Intermetallics* 140: 107392 (2022).

[21] P. Blaha, K. Schwarz, P. Sorantin, and S.B. Trickey. Full-potential, linearized augmented plane wave programs for crystalline systems. *Computer Physics Communications* 59: 339-415 (1990). https://doi.org/10.1016/0010-4655(90)90187-6.

[22] P. Blaha, K. Schwarz, G.K.H. Madsen, D. Kvasnicka, and J. Luitz. WIEN2K, An Augmented Plane Wave Local Orbitals Program for Calculating Crystal Properties. *Vienna University Technology, Vienna, Austria* (2001).

[23] P. Kepple, and H.R. Griem. Improved stark profile calculations for the hydrogen lines Hα, Hβ, Hγ, and Hδ. *Physical Review* 173: 317 (1968). https://doi.org/10.1103/PhysRev.173.317.

[24] C.C. Kim, J.W. Garland, H. Abad, and P.M. Raccah. Modeling the optical dielectric function of semiconductors: Extension of the critical-point parabolic-band approximation. *Physical Review B* 45: 11749 (1992). https://doi.org/10.1103/PhysRevB.45.11749.

[25] R. de L. Kronig. On the Theory of Dispersion of X-Rays. *Journal of the Optical Society of America* 12: 547-557 (1926). https://doi.org/10.1364/josa.12.000547.

[26] E. Haque, and M.A. Hossain. Structural, elastic, optoelectronic and transport calculations of Sr3SnO under pressure. *Materials Science in Semiconductor Processing* 83: 192-200 (2018). https://doi.org/10.1016/j.mssp.2018.04.037.